CHARACTERIZATION OF SIMPLIFIED MULTILAYER BIOSENSOR WITH CONDUCTIVE POLYTHIOPHENE DERIVATIVE POLYMER ON MYELIN BASIC PROTEIN DETECTION

by

Junhao Liang

A thesis submitted to Johns Hopkins University in conformity with the requirements for the degree of Master of Science in Engineering

Baltimore, Maryland

May 2021

Abstract

This essay reports on the fabrication and characterization of a simplified multilayer biosensor with conductive polythiophene derivative polymer (PT-COOH) on myelin basic protein detection. The topic is worth investigation due to the increasing interest and clinical need for label-free real-time protein detection in the healthcare and medical diagnosis area. The first objective of this work is to fabricate a stable biosensor platform that allows the reaction and crosslinking of the myelin basic protein (MBP) and its antibody (anti-MBP) on the polymer film. A second objective is to investigate the connection between the surface zeta potential of the biosensor and the existence of the myelin basic protein in an aqueous environment. The goal is to relate the surface zeta potential change as a sign for the myelin basic protein detection.

To improve the water stability of the polythiophene derivative polymer film, we functionalized the glass substrate with (3-Aminopropyl) triethoxysilane (APTES) silanization for 1 hour before spin-coating the polymer solution on the substrate. The advancing contact angles and surface zeta potential for the PT-COOH film remain the same after water immersion for 12 hours.

For the surface zeta potential characterization, the biosensor samples were measured at each of the four stages: (1) PT-COOH film; (2) PT-COOH + Anti-MBP; (3) PT-COOH + Anti-MBP + BSA; (4) PT-COOH + Anti-MBP + BSA + MBP. The result values show a significant change of surface zeta potential after crosslinking the anti-MBP on the PT-COOH film, indicating the effectiveness of the crosslinking between the PT-COOH and anti-MBP. However, a medium signal change is observed after binding the MBP to the biosensor with anti-MBP. It remains

controversial to take the medium signal change as an effective sign of the detection of myelin basic protein. Two possible explanation of the results are also introduced in this work.

Committee: Dr. Joelle Frechette (academic advisor, ChemBE)

Dr. Michael Bevan (ChemBE)

Acknowledgements

To begin with, I want to express my sincere thankfulness to my advisor Dr. Joelle Frechette. It is my honor to be supervised by Joelle and I couldn't appreciate more for her great patience in every detail towards my research. Her encouragements and understandings could always cheer me up when I was stuck with some problems in the research. I could never finish my work by myself without her help.

I also want to say thank you to all the group members who helps me a lot in the past two years. Thanks for Zach's useful suggestions on making good experiment plans and analyzing data. I want to thank Yu for giving me a lot of helps in training devices and taking great microscope images. Thank Xingche for teaching me to make good data plots. Nikki and Preetika also gave me many advise to help me fix the problems. Also I want to thank Paul and Anushka as well. I really learn a lot from you guys.

Finally, I want to thank all my families and friends who gave me great supports and love. The past two years are very special and it would be incredible boring without you. Thank you!

Contents

List of Tables

List of Figures

1. Introduction

Over the past decades, the interest and need for label-free, real-time, low-cost and reliable biosensors continues to rise, especially in the healthcare and medical diagnosis area[1]. Among many kinds of sensors, biosensors that can directly transduce a biological reaction or binding process into an electronic signal in a label-free manner are much more convenient and straightforward in digital readout and data processing[2]. As one of the most popular sensor platforms, organic thin film transistors (OTFTs) have gained considerable attention in the last two decades with advantages in biocompatibility, low power consumption and real-time detection. A wide range of analytes such as gases (NH_3, N_2, O_3, and ethylene), explosive chemical (DNT and TNT) and many biomolecules (DNA, protein, and glucose) could be detected by OTFTs sensor[3-6]. By introducing a specific detection layer on the OTFT surfaces, analytes can be identified after binding or reacting with the biosensor. Many non-molecular materials such as silicon nanowires[7,8,17], carbon nanotubes[9,10,11,15] and graphene[12] are used and the limitations on these approaches can include their cost and relatively arduous fabrication procedure.

As an alternative to the conventional inorganic-based devices, organic polymer materials provide a unique combination of electronic, chemical, and mechanical properties which have promising application on the biosensor[18,19,20,21]. Hadayat et al. built Pentacene-based organic thin-film transistors that exhibit fast label-free real-time detection of nanoscale biomolecules with a high affinity constant at pH 7 and a high degree of discrimination in the hybrid anti-BSA charges[13]. Magliulo et al. built poly(3-hexylthiophene-2,5-diyl) (P3HT) based organic field-effect transistor sensors with supported biotinylated phospholipid bilayer and created a general platform for EGOFET biosensing demonstrating that proper bio-functionalization can lead to stable and reliable

label-free electronic sensing in aqueous solution[14]. Implementation of polymers with polar functional group moieties such as carboxylic groups can help control selectivity and enhance sensitivity of the OTFT sensors. For example, Dong et al. enhanced the sensor response for individual detection towards CO and NH_3 gases by functionalizing single-walled carbon nanotubes with carboxylic groups[15]. Yang et al. built a thin-film field-effect transistor-based sensor for ammonia and other amines with remarkable high sensitivity and satisfactory selectivity by introducing carboxylic acid groups in dipyrrolopyrrole (DPP) – bithiophene conjugated OTFT polymers[16].

Myelin Basic Protein (MBP) is the second most abundant myelin protein and comprises the myelin sheath which is necessary for the normal activity of the nerve system. MBP concentration can increase in serum in response to central nervous system injury or disorder such as multiple sclerosis[22-25]. At present, there is a clinical need to detect MBP in serum accurately in real time for central nerve system injury diagnose.

In this work, we build simplified organic thin-film transistor biosensor using a conductive polymer Poly [3-(3-carboxypropyl)thiophene-2,5-diyl] regioregular (PT-COOH) to detect Myelin Basic Protein (MBP). As shown in Figure 1, the structure of the simplified biosensor consists of three layers: silica slide substrate, a receptor layer of PT-COOH and an immobilized layer of anti-Myelin Basic Protein antibody (Anti-MBP). After adding MBP protein solution on top of the biosensor, a specific binding between Anti-MBP and MBP would occur. In order to quantify the surface electrical property before and after anti-MBP and MBP binding on the device, we measure the surface zeta potential using dynamic light scattering (DLS) technique.

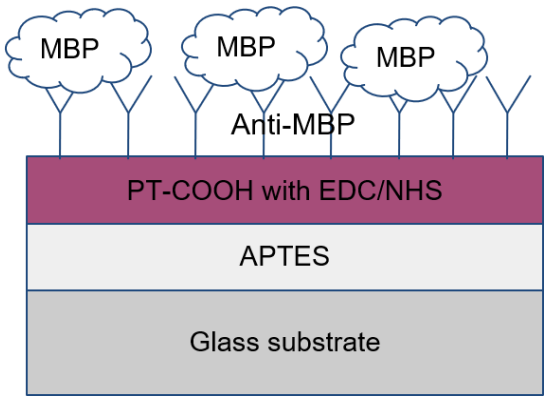

Figure 1. A brief schematic of the simplified biosensor.

2. Theory

2.1 Mechanism and calculation of surface zeta potential

The majority of particle and solid surfaces in aqueous systems are always charged, no matter positively or negatively. Regardless of their charges, the surface charge of particle and solid surface would be neutralized by an adjacent ions layer in the aqueous solution with opposite charge to the surface. Figure 2 is a brief schematic of the electrical diffuse double layer structure in the Gouy-Chapman double layer model. At equilibrium, a balance would be established between the surface charge and the counterions closed to the surface. The counterions structure could be divided into two layers: the inner Stern layer where counterions closely adsorb to the surface and the diffuse layer where the concentration of counterions decreases against distance to the surface[34,35]. The combination of the surface charge and the counterions would produce a variation of the potential in the solution, $\psi(x)$, which changes from the surface potential ψ_0 to zero at a far distance away from surface[36].

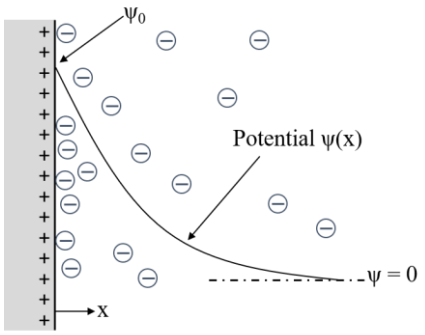

Figure 2. The Gouy-Chapman diffuse double layer model.

We follow closely the approach from Berg's *An Introduction to interface & colloids: the bridge to nanoscience*[34] and Hunter's *Zeta potential in colloid science: principle and applications*[35].

Poisson's equation is used to describe the potential profile in the diffuse part of the electrical double layer:

$$\nabla^2\psi = -\frac{1}{\varepsilon\varepsilon_0}\rho_e \tag{1}$$

where ψ is the local potential, ε is the relatively permittivity of the medium, ε_0 is the permittivity of free space, ρ_e is the space charge density.

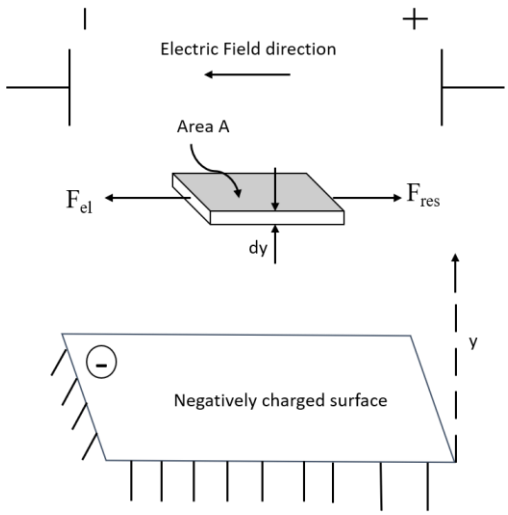

Figure 3. Force diagram of electro-osmotic flow.

The electro-osmosis process would occur when an electrical field applied parallel to the charged surface. Assuming a negatively charged surface, there will be the movement of positively charged counterions in the adjacent liquid towards cathode of the applied field, which will draw the liquid along with them. Hence, an electro-osmotic fluid flow would show up near the charged surface. A force balance could be drawn on a thin control volume in the electro-osmotic flow as

shown in figure 3. Two forces are in balance in the steady state: electrical stresses F_{el} and viscous resistance F_{res}.

The electrical force is due to the applied electric field on the net positive charge within the control volume:

$$F_{el} = qE_x = \rho_e dV E_x \tag{2}$$

where $dV = Ady$ is the volume value of the control volume, ρ_e is the charge density, E_x is the imposed electric field.

By replacing ρ_e with the one-dimensional Poisson equation (1), equation (2) will turn into:

$$F_{el} = \left(-\varepsilon\varepsilon_0 \frac{d^2\psi}{dy^2}\right) AdyE_x \tag{3}$$

the resisting counter force in the x direction comes from the viscous resistance:

$$F_{res} = Ad\tau_{yx} = A\frac{d\tau_{yx}}{dy}dy \tag{4}$$

and according to the Newton's law of viscosity, the viscous shear stress for a Newtonian fluid is:

$$\tau_{yx} = -\mu\frac{dv_x}{dy} \tag{5}$$

where μ is the fluid viscosity.

Combining equation (4) and (5) gives:

$$F_{res} = -A\mu\frac{d^2V_x}{dy^2}dy \tag{6}$$

and equating the electrical force and the resistance force at steady state:

$$\left(-\varepsilon\varepsilon_0 \frac{d^2\psi}{dy^2}\right) AdyE_x = -A\mu\frac{d^2V_x}{dy^2}dy \tag{7}$$

Here equation (7) can be integrated twice with the following boundary conditions:

$$\begin{cases} \text{when y} \to \infty \text{ (far away from the surface)}, \dfrac{dv_x}{dy} = \dfrac{d\psi_x}{dy} = 0 \\ \text{when y} \to 0 \text{ (the “slip plane”)}, V_x = 0 \end{cases}$$

The result of electro-osmotic velocity V_e is:

$$V_e = -\frac{\varepsilon\varepsilon_0 E_x \zeta}{\mu} \tag{8}$$

Equation (8) gives the relationship between the surface zeta potential ζ and electro-osmotic fluid velocity V_e and it is the basic of the surface zeta potential measurement technique. Here the negative sign in the equation (8) indicates that when the surface zeta potential ζ is negative (negatively charged surface with positive counterions in the double layer), then the V_x is positive and the liquid flow is moving towards the negative electrode.

Note that no special assumptions are made about the potential distribution in the electrical diffuse double layer and the integration is carried out from the bulk solution to the slip plane. Therefore, the details of the potential distribution between the solid surface and the slip plane have nothing to do with the result.

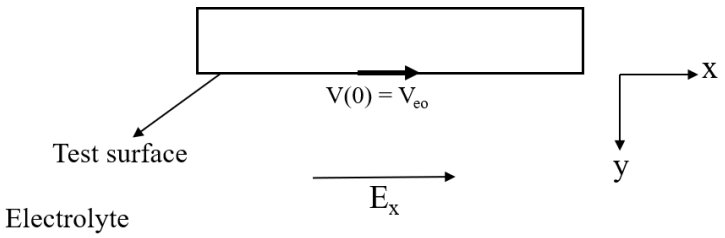

Figure 4. Schematic diagram of the elecroosmotic flow geometry

Now with equation (8), the surface zeta potential ζ could be easily converted once knowing the fluid velocity V_e. Figure 4 shows the electroosmotic flow geometry of a single charged surface in an electrolyte with an external applied electric field. The surface zeta potential in the electrolyte,

the applied electric field and the presence of hydrated ionic species within the electrolyte cause electroosmotic fluid motion along the surface's slipping plane[26].

Assuming Stokes flow and zero back-pressure, we have the linearized Navier-Stokes equation:

$$\rho\dot{v} = \mu\left[\frac{\partial^2 v}{\partial \mathrm{x}^2} + \frac{\partial^2 v}{\partial \mathrm{y}^2}\right] \tag{9}$$

where v(t, x, y) is the component of the fluid velocity parallel to the boundary, ρ is the fluid density and μ is the fluid viscosity. Because there is no flow perpendicular to the boundary, velocity v is not a function of x and the equation (9) could simplify to:

$$\dot{v} = k\left[\frac{\partial^2 v}{\partial \mathrm{y}^2}\right] \tag{10}$$

where $k = \frac{\rho}{\mu}$. Combined with the initial condition v(0,y)=0, boundary condition v(t,0)=V_e where V_e is the fluid velocity at the boundary, homogeneous initial conditions and Dirichlet boundary conditions on the half line (0, ∞) and a Green function solution, equation (10) could be expressed in closed form as follows:

$$v(y,t) = \int_0^\infty \frac{1}{\sqrt{4\pi k(t-s)^3}} exp\, \frac{y^2}{4k(t-s)} V_e ds \tag{11}$$

This has the following closed form solution:

$$v(y,t) = V_e\left[1 - erf\left(\frac{y}{2\sqrt{kt}}\right)\right] \tag{12}$$

where erf is the error function. For water at 25°C, the term in square brackets in equation (12) disappears at y ≥ 750um for t ≥ 75ms or y ≥ 1.5mm for t ≥ 300ms. Therefore, as shown in figure 5, a fit of equation (12) to measurements of $v_i(y_i)$ at various points y_i can then be extrapolated to

the y-axis intercept to yield V_e, which can be used to calculate the surface zeta potential ζ by equation (8).

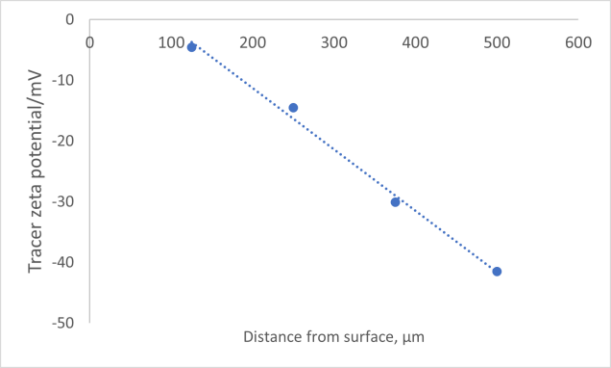

Figure 5. A typical measurement plot of particle average zeta potential against displacement from surface.

2.2 Anti-Myelin Basic Protein (MBP) antibody binding chemistry

Few chemical groups are able to create effective conjugation between carboxylic acids group (-COOH) and biomolecules like proteins. While carbodiimide compounds provide the most popular and versatile method for crosslinking to carboxylic acids. The most commonly used one is the water-soluble EDC (1-ethyl-3-(-3-dimethylaminopropyl) carbodiimide hydrochloride) for aqueous crosslinking. Also, NHS (N-hydroxysuccinimide) is often included in the EDC crosslinking protocols, which could improve the reaction efficiency and create dry-stable (amine-reactive) intermediates.

EDC/NHS chemistry is well-established in organic and bioconjugate chemistry and is applicable for both solution and solid surface[27]. Figure 6 is the EDC/NHS crosslinking reaction scheme. The crosslinking agent EDC used to couple carboxylic groups to primary amines via the

formation of amine-reactive NHS-esters. EDC firstly react with carboxylic acid group to form an active but water-unstable O-acylisourea intermediate. When this intermediate doesn't meet an amine, it will hydrolyze and regenerate the carboxylic group and lower the crosslinking efficiency. In the presence of NHS, EDC couples NHS to carboxylic acid group and form an NHS ester that considerably more stable in the solution, allowing for better conjugation to the antibody itself[28].

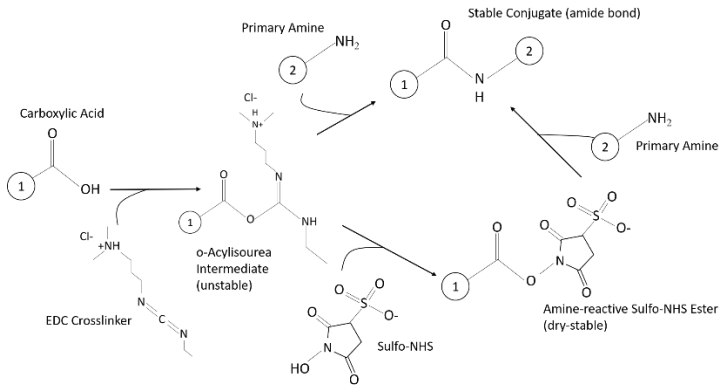

Figure 6. Reaction scheme of EDC/NHS crosslinking chemistry[27].

2.3 Functionalization of silica surface with liquid phase APTES silanization

The water stability of PT-COOH film is the prerequisites of the following crosslinking between polymer film and anti-MBP. However, the binding between PT-COOH film and bare silica surface is too weak to ensure its water stability. The film would fall off from the silica surface and stop remain intact. Hence it is essential to functionalize the silica surface with aminosilanes in solution phase and provide extra binding between the polymer and the surface.

(3-Aminopropyl)triethoxysilane (APTES) is an aminosilane frequently used in the process of silanization and could be used to functionalize silica surfaces[29,30]. As shown in figure 7, by applying APTES on the silica surface, bonding between APTES molecules and silicon oxide substrates occurs, which would introduce amine group (-NH_2) on the silica surface. After the solution phase silanization, the polymer film has significantly improvement in the water stability and would not fall off from the silica surface even after immersing in water over 48 hours.

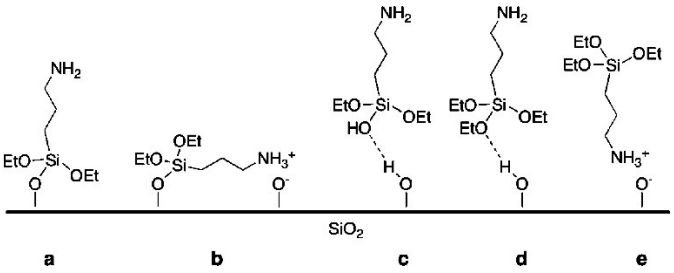

Figure 7. Different types of interactions between APTES molecules and silicon dioxide substrates: (a) a covalently attached APTES molecule with its amine group extending away from the interface, (b) a covalently attached APTES molecule with its amine group interacting with a surface silanol group, and (c–e) weakly bounded APTES molecules[29].

3. Methods

3.1 Materials, chemicals, equipment and instruments

Table 1. Materials, chemicals equipment and instruments applied in the experiments

Chemicals and materials	Distributor
(3-Aminopropyl)triethoxysilane (APTES)	Sigma-Aldrich
N,N-Dimethylformamide (DMF)	Sigma-Aldrich
Sulfuric acid (98%)	J.T.Baker from Avantor
Hydrogen peroxide	Fisher scientific
Toluene	Fisher scientific
Anhydrous toluene	Sigma-Aldrich
Deionized (DI) water	Milli-Q Academic water purification system
Poly [3-(3-carboxypropyl)thiophene-2,5-diyl] regioregular	Rieke metals
Phosphate buffered saline (PBS)	Sigma-Aldrich
N-Hydroxysuccinimide (NHS)	Sigma-Aldrich
1-ethyl-3-(-3-dimethylaminopropyl) carbodiimide hydrochloride (EDC)	Sigma-Aldrich
Anti-Myelin Basic Protein (MBP) antibody	Sigma-Aldrich
Myelin Basic Protein (MBP)	Sigma-Aldrich
Bovine Serum Albumin	Sigma-Aldrich
FITC conjugated Anti-MBP antibody	Biorbyt
Microscope slides (25x75x1.0mm)	Fisher scientific
Equipment and instruments	**Brand**
Zetasizer Nano ZS	Malvern Panalytical (UK)
Surface zeta potential accessory (ZEN1020)	Malvern Panalytical (UK)

3.2 Preparation of simplified biosensor samples

3.2.1 Glass substrate preparation

Step 1: Cleaning. 7mm x 4mm glass slides and petri dishes are cleaned in Piranha solution (98% sulfuric acid: 30% hydrogen peroxide = 4:1) for over an hour, then wash them clean with deionized water and blow dry them with nitrogen gas. Leave the clean slides and dishes in the laminar flow hood to avoid dust.

Step 2: O2 plasma treatment. Put the clean glass slides into the plasma device chamber, follow the O2 plasma treatment procedures and treat the slides for 2 min.

Step 3: APTES silanization. Immerse the clean glass slides into the anhydrous toluene/APTES solution (50ml/ml) and react for 1hour in the desiccator. Then rinse them twice with toluene, ethanol and deionized water. Bake and dry the slides in the oven at 110℃ for 15 minutes.

3.2.2 Preparation of the PT-COOH/DMF solution

Step 1: PT-COOH powder is weighed in the electronic scales and put into two vials. Dimethylformamide (DMF) is added into each vial using 1000ul pipette. The concentration ratio of PT-COOH and DMF is 20mg/ml.

Step 2: To better disperse the PT-COOH particle, the vial should be under sonication for 5 minutes. There should still be a lot of particles visible to the naked eye after sonication.

Step 3: Vials of PT-COOH/DMF solution are heated on the heat plate at 130 ℃ for 15 min. The solution should be more viscid after heating.

Step 4: The PT-COOH & DMF solution in the new vial is filtered through a 0.20um PTFE filter. The solution will lose a few of its value after filtering and should be put into a new vial.

3.2.3 Preparation of the PT-COOH samples by spin-coating

Step 1: Attach the APTES/glass substrate on another glass substrate with a piece of double-sided tape.

Step 2: Apply 10ul of PT-COOH/DMF solution on each APTES/glass substrate and spin-coat at 3000RPM for 30s.

Step 3: Bake the samples on the heat plate at 90℃ overnight to remove the residual solvent.

3.2.4 Activation of the PT-COOH surface with EDC/NHS/deionized water solution

Step 1: EDC/NHS/DI water solution preparation: dissolve EDC in DI water and then add NHS into EDC/DI water solution. The concentration ratio of EDC/DI water is 10mg/ml, of NHS/DI water is 3mg/ml.

Step 2: Apply 10ul of EDC/NHS/DI water solution on each sample and react at room temperature for 30 minutes. Then wash them carefully with deionized water for five times to remove the excess EDC/NHS solution and blow dry the surface with nitrogen gas.

3.2.5 Antibody immobilization on the PT-COOH surface

Step 1: Apply 10μl of anti-Myelin Basic Protein (Anti-MBP, 100 μg/ml in 1xPBS) solution on sample surface for 3 hours in a humid environment. In order to avoid water evaporation and antibody contamination, the biosensor samples are stored in a humid petri dishes during the

reaction. Then gently wash the samples five times with PBS solution to remove any noncovalently bound antibodies on the surface.

3.2.6 Attachment of protein on the biosensor sample

Step 1: Add 10ul of bovine serum albumin (BSA, 10mg/ml in 1xPBS) on the anti-MBP immobilized surface and wait for half an hour. Then wash them carefully with PBS solution for five times to remove the excess BSA. Theoretically, the BSA will only attach to the sample surface without binding to the anti-MBP.

Step 2: Apply 10µl of Myelin basic protein (MBP, 10 µg/ml in 1xPBS) solution on sample surface for 20 minutes. Then wash five times gently with PBS solution to remove unbinding MBP on the surface. Because of the existence of BSA, MBP can only have specific reaction with anti-MBP without having other noncovalently bound reaction on the surface.

3.3 Surface zeta potential (SZP) measurements

The 7mm x 4mm biosensor sample are attached to the sample holder with 3M VHB tape for the surface zeta potential (SZP) measurement using Malvern Zetasizer NanoZS surface zeta potential accessory (ZEN1020). The tracer particles solution is prepared by dispersing 5ul of sulfate latex particles in 40ml dilute phosphate buffered saline solution (PBS) at pH 7.4. Sulfate latex particles are negatively charged and have a stable zeta potential of -50mV around pH 7.4. Each biosensor sample is immersed in the tracer particles solution during the surface zeta potential measurement.

The Zetasizer equipment uses phase light scattering (PALS) technique to obtain the zeta

potential of the tracer particles at different distances away from the tested sample surface. This technique is based on the Doppler effect and dynamic light scattering. In the aqueous solution, the charged tracer particles are moving under two effects: electroosmotic flow and electrophoresis movement from the applied electronic field. Therefore, the incoming light from the laser will be scattered by the moving tracer particles. According to the Doppler effect, the frequency of outcoming light would change after scattering. As a result, the frequency of incoming and outcoming light is linear to the potential difference between tracer particles and the tested surface[26].

After collecting the apparent tracer particles velocity at different position (125, 250, 375 and 500um), the software then fits them as a function of distance to a straight line. The intercept at zero distance represents the velocity of the tracer particles at the slipping plane of sample surface and can be interpret as the contributions of both electroosmotic and electrophoretic effect ($Intercept = V_{ep} - V_{eo}$). Here V_{ep} is the electrophoretic velocity of tracer particles and can be measurement at the distance 1000um away from the sample surface with no electroosmotic flow. Hence we could obtain the fluid velocity at the slipping plane of the sample surface V_{eo} and convert it into surface zeta potential ζ by equation (8). Each measurement is repeated thrice and average value is reported along with the standard deviation.

4. Results and discussion

4.1 Water stability of the PT-COOH film

As is discussed in chapter 3, after spin-coating the PT-COOH layer on top of the glass substrate, the samples need to be in touch with several aqueous solution such as EDC/NHS water solution, anti-MBP solution and MBP protein solution. Besides, the biosensor samples would immerse in the tracer particles solution during the surface zeta potential measurement. Therefore, it is essential to make sure that the PT-COOH film has a strong water stability and never comes off from the substrate.

Figure 8 shows the images of PT-COOH film after immersing in deionized water for 12 hours with and without the APTES silanization on the glass substrate. The PT-COOH film is very fragile in water if the glass substrate doesn't have any APTES silanization treatment. Based on our observation, the polymer film would easily break into pieces and come off from the substrate, which makes it impossible to bind any anti-MBP on the sample surface. After the glass substrate reacts with APTES for an hour, it is obvious that the PT-COOH film could remain stable and intact in aqueous environment for a long time.

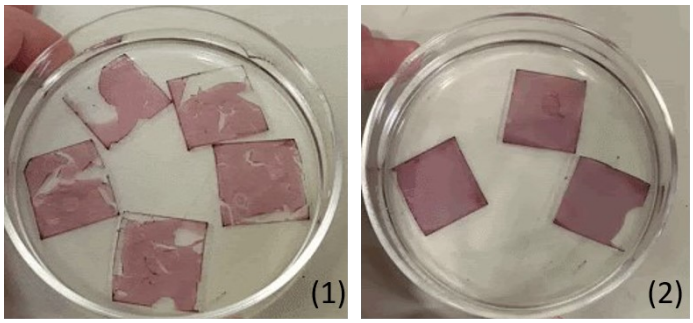

Figure 8. Images of PT-COOH film after immersing in deionized water for 12 hours (1) without APTES silanization; (2) with 1h APTES silanization.

Table 1 shows the advancing contact angles of the PT-COOH film under different APTES silanization time. We control the reaction time between glass substrate and APTES to 1 hour, 3 hours and 6 hours. All the PT-COOH film improve their stability in aqueous solution no matter the reaction time. To further study the influence of the silanization time and the water immersion on the film, we measure the advancing contact angles of PT-COOH film under different reaction time before and after immersing in water for 12 hours. The results show that the water immersion doesn't have an obvious change for the advancing contact angles of the PT-COOH film with 1h and 3h silanization time. There isn't a significant difference in the advancing contact angles value among samples with different reaction time without water immersion. Therefore, one hour APTES reaction time is sufficient enough to meet the needs of the water stability improvement of the PT-COOH film.

	APTES Reaction time	Before water immersion	After water immersion
Advancing contact angles/°	1h	52.9 ± 3.0	57.9 ± 1.0
	3h	57.3 ± 1.8	55.2 ± 0.7
	6h	54.0 ± 1.4	47 ± 1.1

Table 1. Advancing contact angle for PT-COOH film under different APTES silanization time.

4.2 Surface zeta potential of the simplified biosensor at different stages

To investigate the difference of the simplified biosensor at four different stages, we measure the surface zeta potential value of the biosensor samples at each stage: (1) PT-COOH film; (2) PT-COOH + Anti-MBP; (3) PT-COOH + Anti-MBP + BSA; (4) PT-COOH + Anti-MBP + BSA + MBP. We measure two to three individual batches of samples at each stages to ensure data repeatability. As shown in figure 9 and table 2, surface zeta potential values of different samples are plotted with different colors.

At the initial stage without having any protein or antibody on the surface, the PT-COOH film has a surface zeta potential of -76.6 ± 2.2mV. After binding the anti-MBP on the PT-COOH film, we observe a clear increasement of surface zeta potential and the result value is -44.1 ± 6.5mV. The signal change before and after anti-MBP binding indicates the effectiveness of the crosslinking between the PT-COOH and antibody. Bovine serum albumin (BSA) is then applied on the sample surface. Theoretically, bovine serum albumin will only attach to the sample surface by electrostatic or steric forces without covalently binding to the anti-MBP. Therefore, MBP protein should have a specific reaction with the anti-MBP instead of having non-covalently binding to the sample surface. The addition of bovine serum albumin doesn't change the surface zeta potential and the value is -43.9 ± 6.0mV. The last stage of the biosensor is to let MBP protein spontaneously react with anti-MBP antibody on the surface for 20 minutes. After the binding of MBP protein on the sample, the average surface zeta potential slightly decreases to -48.1 ± 3.8mV. A medium change of average surface zeta potential is obtained after the binding of MBP protein.

However, it remains controversial to connect the medium signal change to the effective

detection of myelin basic protein. Unlike the significant surface zeta potential change after crosslinking the anti-MBP on the film, the signal change from the MBP protein is mediocre. Also, the change in average surface zeta potential is within the error of the measurement. Another controversy is, the myelin basic protein has an overall positive charge at physiological pH of 7.4[31], so the average surface zeta potential of the sample surface should increase toward positive direction after having MBP protein on the biosensor. While the experiment result shows a decreasing signal change after the binding of MBP.

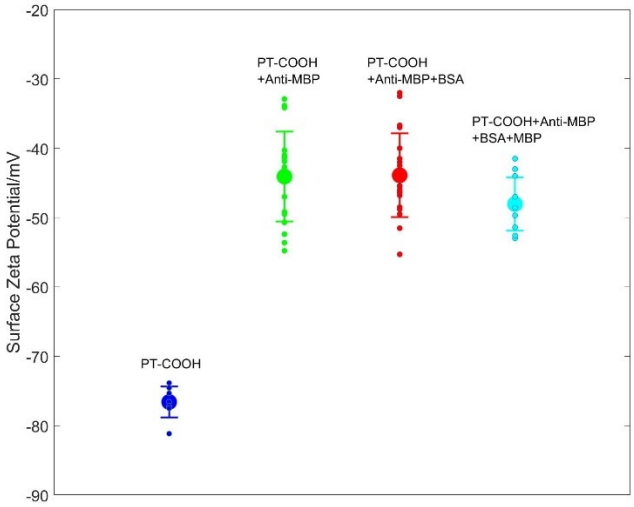

Figure 2. Surface zeta potential value of the simplified biosensor at different stages.

	PT-COOH	PT-COOH + Anti-MBP	PT-COOH + Anti-MBP + BSA	PT-COOH + Anti-MBP + BSA + MBP
Surface zeta potential/mV	-76.6 ± 2.2	-44.1 ± 6.5	-43.9 ± 6.0	-48.1 ± 3.8

Table 2. Summary of surface zeta potential value of the biosensor at different stages

4.3 Possible explanations

To explain the reason of the mediocre signal change by the myelin basic protein, we need to look into the details during the surface zeta potential measurement. Figure 10 is the schematic diagram of the biosensor during the surface zeta potential measurement. The biosensor is immersed in the aqueous tracer solution with negatively charged sulfate latex particles everywhere, so it's possible that the negatively charged tracer particles attach to the positively charged myelin basic protein by electrostatic forces and cancel out the signal change of the surface brought by the protein. Unfortunately, positively charged tracer particles would have a stronger electrostatic interaction with the surface due to the fact that the entire biosensor is negatively charged, while neutral tracer particles would aggregate by themselves under the effect of Van der Waal attraction force.

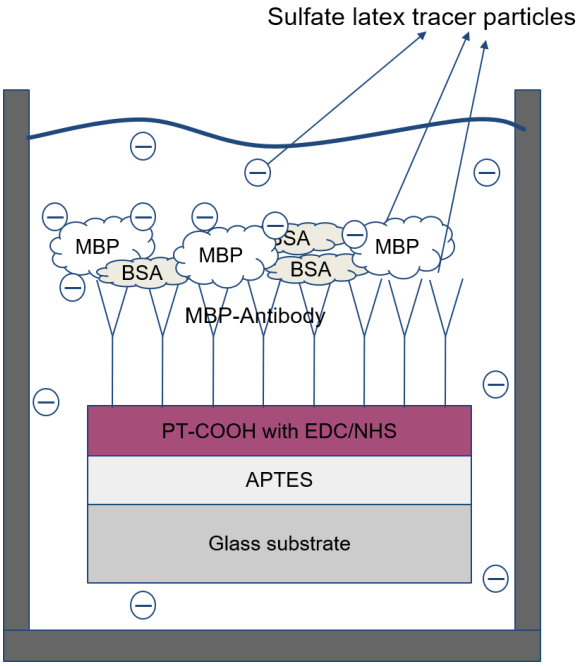

Figure 10 Schematic diagram of the biosensor during the surface zeta potential measurement.

Another explanation of the mediocre signal difference could be the poor-dispersed and insufficient anti-MBP antibody and MBP protein on the biosensor. To have a better understanding towards the crosslinking efficiency of the anti-MBP to the PT-COOH film, we treat the polymer layers with FITC-labeled anti-MBP and take fluorescence images. The results are shown in figure 11. According to the bare glass sample picture, there is hardly any antibody immobilized on the substrate, indicating low nonspecific binding. After FITC labeled anti-MBP is applied to PT-COOH film layer, visible fluorescence is observed. However, the intensity of the fluorescence for PT-COOH sample is medium. Fluorescence quenching of functionalized polythiophenes could be the reason for the medium fluorescence intensity[32].

The fluorescence image for the PT-COOH film could indicate the poor-dispersed anti-MBP on the biosensor. The crosslinking of the anti-MBP on the PT-COOH film has a significant effect on the surface zeta potential change, but the dispersion of the anti-MBP plays an important role in the following MBP protein binding. As shown in figure 12, insufficient and poor-dispersed anti-MBP on the biosensor surface could weaken the binding between anti-MBP and MBP protein, hence minimizing the impact of the MBP on the surface zeta potential of the biosensor.

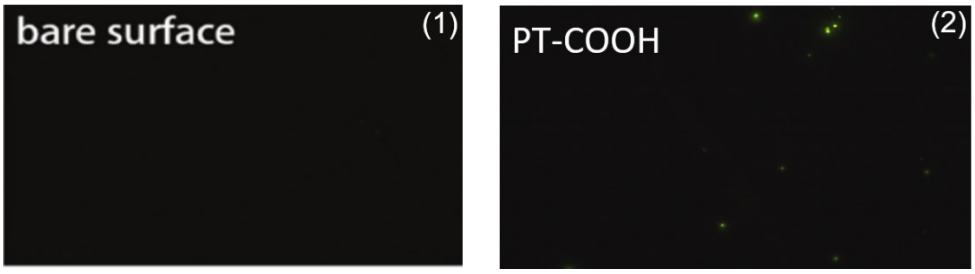

Figure 11. The fluorescence images for FITC label anti-MBP on (1) bare glass surface[33] and (2) PT-COOH

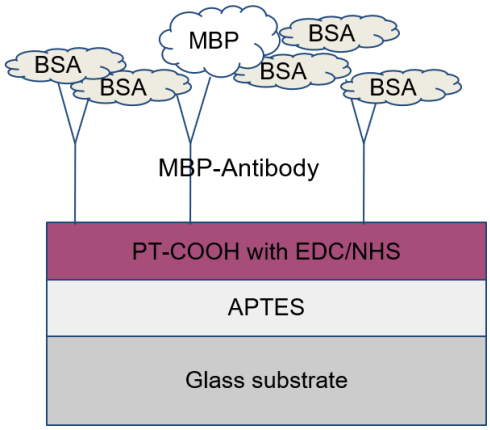

Figure 12. Schematic diagram of the biosensor with insufficient anti-MBP antibody and MBP protein

5. Conclusions

This work mainly focused on the fabrication and surface zeta potential characterization of the multilayer biosensor with polythiophene derivative polymer (PT-COOH). We measured the surface zeta potential change of the biosensor after binding with anti-myelin basic protein antibody (anti-MBP) and myelin basic protein (MBP). The goal is to relate the surface zeta potential change as a sign for the myelin basic protein detection.

A stable polymer film platform is the prerequisite for the following anti-MBP and MBP binding reaction on the biosensor. The PT-COOH polymer film is extremely fragile in aqueous solution when spin-coating on the bare glass substrate. Functionalization of glass substrate with 1 hour liquid phase APTES silanization has proved to be an effective method to improve the water stability of the PT-COOH film. The water immersion has little influence on the advancing contact angles and surface zeta potential of the polymer film with silanization treatment.

Surface zeta potential (SZP) for each layer of the biosensor was measured. After the anti-MBP binding to the PT-COOH film, we observed an significant change in the surface zeta potential value, indicating the effective crosslinking between the antibody and the polymer. The biosensor has a clear response towards the anti-MBP binding. Based on the biosensor with anti-MBP, bovine serum albumin (BSA) and myelin basic protein were added on the biosensor surface individually. However, there was only a medium change of the surface zeta potential for the BSA samples and the MBP samples comparing to the anti-MBP samples. It remains controversial to take the medium signal change as an effective sign of the detection of myelin basic protein.

There are two explanation of the unsatisfied surface zeta potential change for the MBP samples. Firstly, the myelin basic protein has an overall positive charge at physiological pH. During the surface zeta potential measurements, the negatively charged sulfate latex particles could stick on the MBP protein under the electrostatic force, which cancel out the signal change of the surface brought by the MBP protein. Another explanation of the mediocre signal difference could be the distribution of anti-MBP antibody and MBP protein on the biosensor. The mediocre fluorescence intensity of the FITC labeled anti-MBP antibody on the PT-COOH film indicated a poor-dispersed and insufficient amount of anti-MBP on the biosensor, which weakened the binding between anti-MBP and MBP protein and minimized the impact of the MBP on the surface zeta potential of the biosensor.

6. Reference

1. Yager, P., Domingo, G. J., & Gerdes, J. (2008). Point-of-care diagnostics for global health. *Annual review of biomedical engineering*, *10*.
2. Roberts, M. E., Sokolov, A. N., & Bao, Z. (2009). Material and device considerations for organic thin-film transistor sensors. *Journal of Materials Chemistry*, *19*(21), 3351-3363.
3. Huang, W., Besar, K., LeCover, R., Rule, A. M., Breysse, P. N., & Katz, H. E. (2012). Highly sensitive NH3 detection based on organic field-effect transistors with tris (pentafluorophenyl) borane as receptor. *Journal of the American Chemical Society*, *134*(36), 14650-14653.
4. Bouvet, M., Xiong, H., & Parra, V. (2010). Molecular semiconductor-doped insulator (MSDI) heterojunctions: oligothiophene/bisphtalocyanine (LuPc2) and perylene/bisphthalocyanine as new structures for gas sensing. *Sensors and Actuators B: Chemical*, *145*(1), 501-506.
5. Esser, B., Schnorr, J. M., & Swager, T. M. (2012). Selective detection of ethylene gas using carbon nanotube-based devices: utility in determination of fruit ripeness. *Angewandte Chemie International Edition*, *51*(23), 5752-5756.
6. Huang, W., Besar, K., LeCover, R., Rule, A. M., Breysse, P. N., & Katz, H. E. (2012). Highly sensitive NH3 detection based on organic field-effect transistors with tris (pentafluorophenyl) borane as receptor. *Journal of the American Chemical Society*, *134*(36), 14650-14653.

7. Das, Arindam, et al. "A nitrogen dioxide sensor based on an organic transistor constructed from amorphous semiconducting polymers." *Advanced Materials* 19.22 (2007): 4018-4023.
8. Shen, F., Wang, J., Xu, Z., Wu, Y., Chen, Q., Li, X., ... & Zhu, T. (2012). Rapid flu diagnosis using silicon nanowire sensor. *Nano letters*, *12*(7), 3722-3730.
9. Lerner, M. B., D'Souza, J., Pazina, T., Dailey, J., Goldsmith, B. R., Robinson, M. K., & Johnson, A. C. (2012). Hybrids of a genetically engineered antibody and a carbon nanotube transistor for detection of prostate cancer biomarkers. *Acs Nano*, *6*(6), 5143-5149.
10. Liu, S., & Guo, X. (2012). Carbon nanomaterials field-effect-transistor-based biosensors. *NPG Asia Materials*, *4*(8), e23-e23.
11. Allen, B. L., Kichambare, P. D., & Star, A. (2007). Carbon nanotube field-effect-transistor-based biosensors. *Advanced Materials*, *19*(11), 1439-1451.
12. Park, S. J., Kwon, O. S., Lee, S. H., Song, H. S., Park, T. H., & Jang, J. (2012). Ultrasensitive flexible graphene based field-effect transistor (FET)-type bioelectronic nose. *Nano letters*, *12*(10), 5082-5090.
13. Khan, H. U., Jang, J., Kim, J. J., & Knoll, W. (2011). In situ antibody detection and charge discrimination using aqueous stable pentacene transistor biosensors. *Journal of the American Chemical Society*, *133*(7), 2170-2176.
14. Magliulo, M., Mallardi, A., Mulla, M. Y., Cotrone, S., Pistillo, B. R., Favia, P., ... & Torsi, L. (2013). Electrolyte-Gated Organic Field-Effect Transistor Sensors Based on Supported Biotinylated Phospholipid Bilayer. *Advanced Materials*, *25*(14), 2090-2094.

15. Dong, K. Y., Choi, J., Lee, Y. D., Kang, B. H., Yu, Y. Y., Choi, H. H., & Ju, B. K. (2013). Detection of a CO and NH 3 gas mixture using carboxylic acid-functionalized single-walled carbon nanotubes. *Nanoscale research letters*, *8*(1), 1-6.

16. Yang, Y., Zhang, G., Luo, H., Yao, J., Liu, Z., & Zhang, D. (2016). Highly sensitive thin-film field-effect transistor sensor for ammonia with the DPP-bithiophene conjugated polymer entailing thermally cleavable tert-butoxy groups in the side chains. *ACS applied materials & interfaces*, *8*(6), 3635-3643.

17. Lin, T. W., Hsieh, P. J., Lin, C. L., Fang, Y. Y., Yang, J. X., Tsai, C. C., ... & Chen, Y. T. (2010). Label-free detection of protein-protein interactions using a calmodulin-modified nanowire transistor. *Proceedings of the National Academy of Sciences*, *107*(3), 1047-1052.

18. Kergoat, L., Piro, B., Berggren, M., Pham, M. C., Yassar, A., & Horowitz, G. (2012). DNA detection with a water-gated organic field-effect transistor. *Organic Electronics*, *13*(1), 1-6.

19. Lai, S., Demelas, M., Casula, G., Cosseddu, P., Barbaro, M., & Bonfiglio, A. (2013). Ultralow voltage, OTFT-based sensor for label-free DNA detection. *Advanced Materials*, *25*(1), 103-107.

20. Kim, Z. S., Lim, S. C., Kim, S. H., Yang, Y. S., & Hwang, D. H. (2012). Biotin-functionalized semiconducting polymer in an organic field effect transistor and application as a biosensor. *Sensors*, *12*(8), 11238-11248.

21. Buth, F., Donner, A., Sachsenhauser, M., Stutzmann, M., & Garrido, J. A. (2012). Biofunctional Electrolyte-Gated Organic Field-Effect Transistors. *Advanced materials*, *24*(33), 4511-4517.

22. Belogurov, A., Zakharov, K., Lomakin, Y., Surkov, K., Avtushenko, S., Kruglyakov, P., ... & Evdoshenko, E. (2016). CD206-targeted liposomal myelin basic protein peptides in patients with multiple sclerosis resistant to first-line disease-modifying therapies: a first-in-human, proof-of-concept dose-escalation study. *Neurotherapeutics*, *13*(4), 895-904.

23. Derkus, B., Bozkurt, P. A., Tulu, M., Emregul, K. C., Yucesan, C., & Emregul, E. (2017). Simultaneous quantification of Myelin Basic Protein and Tau proteins in cerebrospinal fluid and serum of Multiple Sclerosis patients using nanoimmunosensor. *Biosensors and Bioelectronics*, *89*, 781-788.

24. Friess, M., Hammann, J., Unichenko, P., Luhmann, H. J., White, R., & Kirischuk, S. (2016). Intracellular ion signaling influences myelin basic protein synthesis in oligodendrocyte precursor cells. *Cell Calcium*, *60*(5), 322-330.

25. Derkus, B., Emregul, E., Yucesan, C., & Emregul, K. C. (2013). Myelin basic protein immunosensor for multiple sclerosis detection based upon label-free electrochemical impedance spectroscopy. *Biosensors and Bioelectronics*, *46*, 53-60.

26. Corbett, J. C., McNeil-Watson, F., Jack, R. O., & Howarth, M. (2012). Measuring surface zeta potential using phase analysis light scattering in a simple dip cell arrangement. *Colloids and Surfaces A: Physicochemical and Engineering Aspects*, *396*, 169-176.

27. Bart, J., Tiggelaar, R., Yang, M., Schlautmann, S., Zuilhof, H., & Gardeniers, H. (2009). Room-temperature intermediate layer bonding for microfluidic devices. *Lab on a Chip*, *9*(24), 3481-3488.

28. *Carbodiimide CROSSLINKER chemistry*. (n.d.). https://www.thermofisher.com/us/en/home/life-science/protein-biology/protein-biology-learning-center/protein-biology-resource-library/pierce-protein-methods/carbodiimide-crosslinker-chemistry.html.

29. Asenath Smith, E., & Chen, W. (2008). How to prevent the loss of surface functionality derived from aminosilanes. *Langmuir*, *24*(21), 12405-12409.

30. Zhu, M., Lerum, M. Z., & Chen, W. (2012). How to prepare reproducible, homogeneous, and hydrolytically stable aminosilane-derived layers on silica. *Langmuir*, *28*(1), 416-423.

31. Hu, Y., Doudevski, I., Wood, D., Moscarello, M., Husted, C., Genain, C., ... & Israelachvili, J. (2004). Synergistic interactions of lipids and myelin basic protein. *Proceedings of the National Academy of Sciences*, *101*(37), 13466-13471.

32. Ravichandar, R., Thelakkat, M., & Somanathan, N. (2008). Fluorescence quenching of substituted polyperylene with functionalized polythiophenes. *Journal of fluorescence*, *18*(5), 891-898.

33. Song, J., Dailey, J., Li, H., Jang, H. J., Russell, L., Zhang, P., ... & Katz, H. E. (2018). Influence of Bioreceptor Layer Structure on Myelin Basic Protein Detection using Organic Field Effect Transistor-Based Biosensors. *Advanced Functional* Materials, 28(37), 1802605.

34. Berg, J. C. (2010). An introduction to interfaces & colloids: the bridge to nanoscience. World Scientific.

35. Hunter, R. J. (2013). Zeta potential in colloid science: principles and applications (Vol. 2). Academic press.

36. Israelachvili, J. N. (2015). Intermolecular and surface forces. Academic press.